Radiation Physics and Chemistry 229 (2025) 112519

Contents lists available at ScienceDirect

Radiation Physics and Chemistry

journal homepage: www.elsevier.com/locate/radphyschem

Gamma radiation-induced modifications in structural, optical, and electrical characteristics of *p*-NiO/n-Si heterojunction diodes

Ramazan Lok [a,*], Muhsin U. Doğan [a,b], Senol Kaya [a,c], Ugur Soykan [a,d], Cabir Terzioğlu [a,e]

[a] Center of Nuclear Radiation Detectors Research and Applications, BAIBU, Bolu, Turkey
[b] Electronic and Automation Department, Bolu Abant Izzet Baysal University, Bolu, Turkey
[c] Vocational School of Health Services, Bolu Abant Izzet Baysal University, Bolu, Turkey
[d] Yenicaga Yasar Celik Vocational School Bolu Abant Izzet Baysal University, Bolu, Turkey
[e] Physics Department, Bolu Abant Izzet Baysal University, Bolu, Turkey

ARTICLE INFO

Handling Editor: Dr. Chris Chantler

Keywords:
p-NiO/n-Si heterojunction diodes
Gamma irradiation
Thin films
Band gap
Semiconductors

ABSTRACT

This study examines the effects of Co-60 gamma irradiation on the structural, chemical, optical, and electrical properties of *p*-NiO/n-Si heterojunction diodes. Various characterization techniques such as X-ray Diffraction *(XRD)*, Fourier Transform Infrared *(FTIR)* spectroscopy, *UV–Vis* reflectance measurements, and electrical current-voltage *(I–V)* analysis were used to evaluate the changes caused by radiation. The XRD analysis showed that higher radiation doses caused shifts and broadening in the diffraction peak positions, which indicated a reduction in stress and an increase in grain size in the irradiated films. *FTIR* spectra revealed the weakening of *Ni–O–Si* bonds, as well as the emergence of *Ni–O* and *Si–O* stretching vibrations, particularly in film structures exposed to higher doses. Optical analyses demonstrated a decrease in bandgap energy values to 3.40 eV, 3.36 eV, and 3.34 eV due to the band tailing effect related to radiation-induced defects. Electrical measurements indicated a decrease in sheet resistance from 78.4 Ω/sq to 64.4 Ω/sq, changes in the diode's rectification behavior, and an increase in barrier height from 0.79 eV to 0.87 eV with higher radiation doses, while the ideality factor increased from 1.64 to 1.83. These findings highlight the significant effects of gamma irradiation on the structural and electronic properties of heterojunction diode materials and provide valuable insights for the design of radiation-resistant semiconductor devices.

1. Introduction

Semiconductor devices play a crucial role in technologies and are widely used in various applications such as optoelectronic, transistors, capacitors, and solar cells (Akila et al., 2024; Al-Ahmadi, 2020; Gayathri et al., 2024a; Guo et al., 2024; Lök, 2024). Nickel oxide (*NiO*), with its chemical properties, stands out as an important material in the design of these semiconductor devices. Its p-type conductivity enables the *NiO* to carry electric current through hole carriers, making it suitable for use in semiconductor applications such as solar cells and p-n diodes (Chaoudhary et al., 2022; Irwin et al., 2011). The high thermal stability of the *NiO* enables its effective use in high-temperature applications and energy storage systems, particularly in devices such as supercapacitors (Dhas et al., 2020) and lithium-ion batteries (Ata-ur-Rehman et al., 2022; Pai et al., 2024). Additionally, gas sensing capability of *NiO* offers a significant advantage for environmental monitoring and safety applications, enabling the precise detection of toxic gases (Gomaa et al., 2021; Wang et al., 2023). These versatile properties make *NiO* a critical compound in modern materials science and engineering (Hwang and Hwang, 2020; Kalkan, 2025; Kim et al., 2018; Rattana et al., 2016)

In recent years, the study of materials exposed to various radiation doses has gained significant attention as researchers strive to understand radiation-induced mechanisms within materials that is a critical step in advancing the development of radiation-hardened electronic devices. Many studies in this field examine the effects of γ radiation on the structural, morphological, and optical properties of materials (Mande et al., 2019; Saha et al., 2018; Yağci, 2023). Significant structural changes were observed in devices exposed to radiation (Kahraman et al., 2022). These effects, which vary depending on the energy level, are concentrated on two gamma rays emitted by the Co-60 isotope with energies of 1.17 MeV and 1.33 MeV. Below 1 MeV, the photoelectric effect dominates, in the range of 1–2 MeV, the Compton effect prevails,

* Corresponding author.
E-mail address: ramazanlok@ibu.edu.tr (R. Lok).

https://doi.org/10.1016/j.radphyschem.2025.112519
Received 28 October 2024; Received in revised form 3 January 2025; Accepted 6 January 2025
Available online 7 January 2025

and above 5 MeV, the pair production becomes the dominant mechanism (Parks, 2015). These mechanisms can lead to the formation of traps and changes in the distribution of surface charges, causing degradation in device performance. Additionally, the displacement of lattice atoms can lead to the formation of interstitial defects, which can disrupt the material's crystalline structure, reducing crystallinity and increasing defect density (Debelle and Declemy, 2010; Varichenko et al., 1994). Structural distortions can negatively impact the movement of charge carriers at the heterostructure interface (Mirzayev et al., 2018). *NiO*, a p-type semiconductor in the +2 oxidation state of nickel, may have its oxidation state and thus, its chemical reactivity affected by gamma rays (Sayyed et al., 2022; Zhang et al., 2014). Through *FTIR* analyses, the formation of new chemical bonds or alterations in existing bonds can be observed following gamma exposure. These changes may indirectly influence the electrical properties of *NiO* (Ahmed and Sallam, 2024; Jabbar et al., 2024).

These structural changes directly affect important parameters such as the *I–V* characteristics, rectifying behaviours, ideality factor, and barrier height of diodes (Karataş and Türüt, 2006; Omotoso et al., 2015). The ideality factor of the diode can also change due to gamma irradiation (Sharma et al., 2020). The ideality factor is a parameter that measures the actual behaviour of a diode compared to an ideal p-n junction (Karataş and Türüt, 2006; Pillai et al., 2012; Sharma et al., 2020). While this value is close to 1 for an ideal p-n diode, it may increase in devices exposed to gamma radiation, indicating that the increased defects at the interface cause deviations in the rectifying process (Karataş and Türüt, 2006; Pillai et al., 2012). This suggests that the current transport mechanism of the diode has deteriorated, leading to more recombination mechanisms.

Additionally, gamma radiation can cause changes in the Schottky barrier heights (Ashery et al., 2020; Bodunrin and Moloi, 2022). These changes may cause the barrier to increase or decrease depending on the density of defects and charge traps at the interface. An increase in the barrier height can result in reduced current flow, degrading the conduction properties of the device. Conversely, in some cases, radiation may decrease the barrier height and increase the current, which can improve the diode's performance in the short term but may shorten the device's lifespan in the long term (Akay et al., 2018; Bilgili et al., 2019; Karataş and Türüt, 2006; Omotoso et al., 2015; Pastuovic et al., 2014). Teffahi et al. obtained that Co-60 gamma irradiation leads to significant changes in the electrical properties of Schottky diodes, particularly in terms of series resistance and barrier height (Teffahi et al., 2016). The effects of radiation on the structural and electrical properties of devices vary depending on complex mechanisms (Kaymaz et al., 2021). have reported that significant changes were observed in the main electrical parameters of the Al/(ZnO-PVA)/p-Si heterojunction diode with increasing radiation doses. The reverse leakage current (I_R), initially 1.14×10^{-4} A, increased to 1.57×10^{-4} A, which can be attributed to an increase in defect centers. The barrier height (Φ_B) decreased slightly from its initial value of 0.601 eV to 0.575 eV, indicating changes in the carrier barrier caused by radiation. These changes clearly demonstrate the impact of radiation on defect density and carrier transport mechanisms within the diode. On the other hand (Bobby et al., 2014), have reported the leakage current of irradiated Au/n-GaAs Schottky diodes decreased from 1.74×10^{-5} A to 0.50×10^{-5} A, while the barrier height increased from 0.68–0.69 eV to 0.72–0.74 eV. These changes indicate that irradiation balances defect distribution, enhances carrier mobility, and improves transport mechanisms.

Different materials can exhibit different behaviours in radiation environments due to their inherent properties. This highlights the need for novel studies for each material. This study aims to investigate the performance and potential interaction mechanisms of *Pt/p-NiO/n-Si/Al* heterojunction diodes under radiation, which have not been sufficiently explored in the literature. Such studies are of great importance as they contribute to the development of radiation-resistant electronic devices. *NiO* has a wide range of applications in technological fields. It functions as a p-type semiconductor in devices such as photodetectors and solar cells, and due to its antiferromagnetic properties, it is used in magnetic storage devices. It also serves as an anode material in lithium-ion batteries, a component providing high sensitivity in gas sensors, a colour-changing material in electrochromic devices, and a catalyst in chemical reactions. Despite its versatility, studies examining the radiation damage behavior of *NiO* are limited.

Therefore, this study investigates the effects of Co-60 gamma irradiation on the structural, chemical, optical, and electrical properties of *p-NiO/n-Si* heterojunction diodes. The study aims to reveal the relationships between the structural integrity, chemical composition, optical properties, and electrical performance of the heterojunctions, and how these parameters are affected by gamma irradiation. This comprehensive approach seeks to optimize the performance of *p-NiO/n-Si* heterojunctions in various electronic and optoelectronic applications while also filling this gap in the literature.

2. Experimental details

A polished (100) n-type silicon wafer with a resistivity of *1-4* Ω-cm was utilized as the substrate material. The silicon wafer was subjected to the standard *RCA* cleaning procedure to ensure its cleanliness. Following this, the cleaned wafer was placed into an evaporation chamber to facilitate the deposition of *p-NiO*. The target material for this process consisted of granular *NiO* particles, characterized by a purity of 4 N and a particle size ranging from 1 to 4 mm. Prior to the electron beam evaporation, the chamber pressure was maintained below 8.7×10^{-4} Pa. During the deposition of *NiO*, the filament current was set to 20 mA, and the silicon substrate was heated to 100 °C. A semiconducting *NiO* layer approximately 120 nm in thickness was deposited onto the silicon wafer, with the thickness monitored using an Inficon Thickness Monitor. The *NiO/Si* structure was subsequently annealed in a nitrogen atmosphere at 450 °C for 30 min to achieve the desired structural properties, as detailed in a previous study (Kaya, 2020).After annealing, the samples were sectioned into six pieces. Three of these were chosen to complete the diode structure, with the entire backside of these samples coated with aluminum (Al) using a sputtering system. An alloy containing platinum (Pt) was then deposited onto the *NiO* layer. The use of Pt and Al allowed for the formation of ohmic contacts, while only the *p-n* junction exhibited rectifying behavior in the electrical characteristics of the *p-NiO/n-Si* diodes.

All samples were categorized into three groups. Each group consisted of one thin film (*p*-NiO/n-Si) and one diode (Pt/p-NiO/n-Si/Al) structure. The first group was preserved as virgin samples. The remaining samples underwent exposure to two different gamma irradiation doses using a Co-60 gamma irradiator at *TENMAK* in Ankara. The second group was subjected to a low dose of 500 Gy, while the third group received a high dose of 2000 Gy. The doses of 500 Gy and 2000 Gy were chosen to assess heterojunction diode performance under short- and long-term radiation, addressing gaps in high-dose research and aligning with prior studies (Kaya et al., 2018; Kaya and Yilmaz, 2018). The impact of gamma irradiation on the crystallographic properties of the thin films was assessed using *XRD* measurements on the NiO/Si thin films. Changes in the chemical bonding characteristics induced by gamma irradiation were analyzed through *FTIR* spectroscopy. Additionally, reflectance measurements in the *UV*/Vis range were performed using a spectroscopic reflectometer to evaluate the optical changes in the films before and after gamma irradiation exposure. The electrical sheet resistance of the films was measured using a four-point probe system at room temperature. Detailed investigations into the irradiation-induced alterations in the electrical properties of the samples included *I–V* measurements of the heterojunction diodes conducted before and after each irradiation exposure.

3. Results and discussion

3.1. Irradiation effects on structural characteristics

XRD analyses were performed to examine the changes in the crystal structure of thin films exposed to different radiation doses, and measurements are shown in Fig. 1. This technique is a critical method for understanding radiation induced effects on crystalline structure of materials. The observed diffraction peaks were analyzed using the International Centre for Diffraction Data (ICDD) software and matched with (ICDD card No: 71–1179). The sharp diffraction peak at 33°, originating from the silicon substrate, is a widely observed and well-known result in the literature. On the other hand, peaks corresponding to *NiO* showed orientation in the (110), (200), and (220) planes. According to literature reviews, it can be stated that the (200) plane, located around 44°, is dominant (Alagiri et al., 2012; Debelle and Declemy, 2010). However, in some studies, results where dominant the (100) orientation have been reported. Detailed analyses reveal that the (200) peak becomes dominant at annealing temperatures above 400 °C, which is associated with the nucleation process (Kaya, 2020). As shown in Fig. 1, increasing radiation dose did not cause a significant change in the intensity of the (200) peak. However, it was observed that the peak slightly shifted to the right and broadened with increasing dose.

Detailed analysis of these studies suggests that the (200) peak becomes dominant at annealing temperatures above 400 °C, and this is related to the nucleation process (Kaya, 2020), while no significant changes in the intensity were observed in the (200) peaks with increasing radiation dose as clearly seen in Fig. 1. However, the peak slightly shift to the right as the radiation dose increases. In a perfect crystal, when there is no internal strain associated with d-spacing, the atoms have a regular structure, and this structure is consistent with the theoretically predicted d_0 plane spacing, that is, the distance between the reflecting planes in the crystal is constant, and *XRD* patterns confirm this ideal distance. However, when homogeneous strain occurs in the crystal structure, the distances between atoms expand, and the distance between the reflecting planes becomes larger than that of the d_0. In this case, the diffraction lines in the *XRD* pattern shift to lower angles because the larger d-spacing is associated with a lower diffraction angle. In cases of non-uniform (irregular) strain, the atoms in the crystal may compress or expand at different rates. This leads to a broadening and narrowing of the *XRD* peaks, as different regions of the crystal varying levels of strain. During this broadening, multiple small sub-peaks was also be observed within the peaks, which is a result of the strain differences in different regions of the crystal. As can be seen in Fig. 2, the similar behaviour was observed in the (200) peak in Fig. 1. As a result, significant shifts to the right in the *XRD* peaks were observed with increasing radiation dose. The main reason for these shifts is the reduction in the strain level in the material due to the effect of radiation on the crystal structure. Radiation can cause defects and dislocations within the material to reorganize, making the strain distribution more balanced. Unlike the irregular strain structure observed in the non-irradiated samples, a more homogeneous and uniform strain structure was formed in the irradiated samples. Therefore, the balancing effect of radiation on the crystal structure can be considered the primary mechanism behind the peak shift (Khorsand Zak et al., 2011; Lok et al., 2022; Nasiri-Tabrizi, 2014).

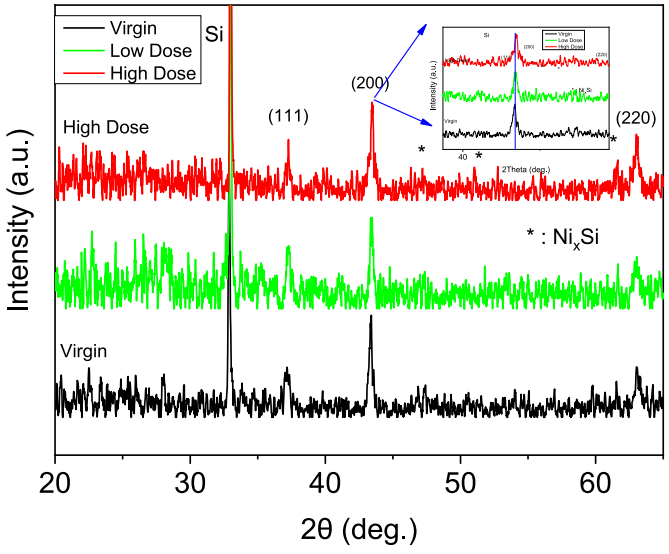

Fig. 1. *XRD* patterns of *NiO* thin films with various radiation doses.

Moreover, the radiation induced effects on the grain size and possible tangent stress associated with grain size fluctuation were calculated via Debye–Scherrer's and tangent correlations given in Ref. (Kaya, 2020). The calculated grain size and tangential strain values are provided in Table 1. In the virgin sample, the crystal size increased from 26.7 nm to 28.5 nm and 32.9 nm with low and high-dose irradiation, respectively, and the lattice strain decreased to 3.52×10^{-3}, 3.29×10^{-3}, and 2.85×10^{-3}. However, the XRD peak broadening does not align with these changes, and this discrepancy is thought to be due to structural defects caused by irradiation. Radiation exposure can lead to microstructural changes, such as phase transformations or variations in particle size, which may be the primary cause of peak broadening (Gayathri et al., 2024b; Omran et al., 2015; Paul et al., 2024; Vinila et al., 2014). The increase in radiation dose likely facilitated the transfer of more energy to the material, enhancing atomic mobility, contributing to the formation of defects like dislocations and vacancies in the crystal structure, and promoting the coalescence of smaller grains into larger ones (Kaya et al., 2019; Madiba et al., 2017). Changes in the grain sizes of the films can be associated with local heating caused by irradiation in nanometer-sized particles. This local heating may also affect the strain-strain relationship between the grains (Hanini et al., 2013; Kaya et al., 2018). Heat may lead to the coalescence of smaller grains into larger clusters. As a result, the reordering of these grains may cause changes in the lattice volume and/or parameters.

3.2. Irradiation effects on chemical bonding characteristics

The *FTIR* spectroscopy measurements were used to determine the effect of gamma-irradiation on *NiO/Si* heterojunction diodes. The mid-infrared spectra of the *NiO/Si* sample with non-irradiated and irradiated with different doses (500 and 2000 Gy) were illustrated in Fig. 3. The absorption bands are located in the low wavenumber finger print region for most metal oxides (Smith, 2018) and hence, the peaks at 556 cm^{-1} is assigned to the *Ni–O* stretching vibrations(Sajilal and Moses Ezhil Raj, 2016). Moreover, *FTIR* spectra taken from the sample before irradiation reveals that the weak bands at ~458 cm^{-1} can be attributed to Ni–*O*–Si bonding in the interface of the *NiO/Si* thin film(Riahi et al., 2017; Sivaiah et al., 2010). The appearance of weak bands belonging to Ni–*O*–Si bond could be an evidence for a chemical bond between *NiO* and *Si* at the interface. This weak absorption band seen at low wavenumber disappeared depending on the dose of gamma-irradiation, while the *Ni–O* stretching vibrations intensity enhanced with rises in the irradiation exposures. In the *IR* spectrum taken after the sample has been exposed to high dose of gamma irradiation, vibrations bands of *NiO* shifted towards high wavenumber with a shoulder at around 614 cm^{-1} are attributed to *Ni–O–H* bending modes. The bands can be also attributed to adsorbed water molecules on the surface of the sample. The broad vibration bands seen around in the range of 700–1100 cm^{-1} of the spectra taken after irradiation with low and high dose of gamma is related to vibration modes of Si–O stretching and bending(Riahi et al., 2017; Sivaiah et al., 2010). In the *IR* spectrum of the heterojunction diode taken after high dose gamma rays, the bending (Riahi et al., 2017) and stretching (Sivaiah et al., 2010) vibration modes of *Si–O–Si*

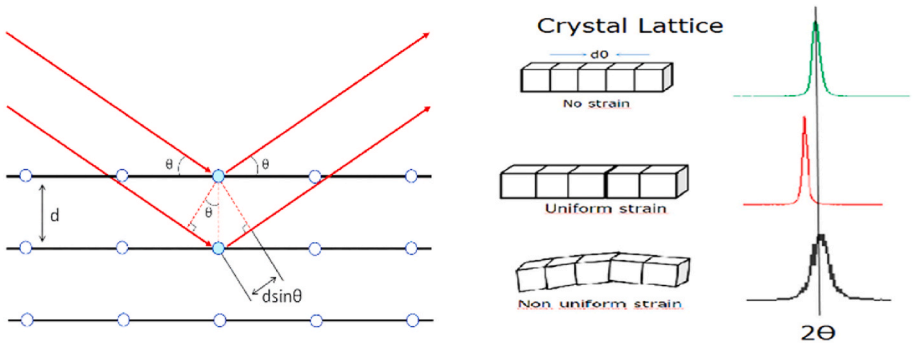

Fig. 2. The effect of strain on the direction of *XRD* patterns of the irradiated samples (Lok et al., 2022).

Table 1
Grain size, lattice strain, and band gap changes.

Sample	2θ (Degree)	Grain Size (nm)	Lattice strain x10^{-3}	Band Gap (eV)
Virgin	43.37	26.7	3.52	3.40
Low D.	43.41	28.5	3.29	3.36
High D.	43.48	32.9	2.85	3.34

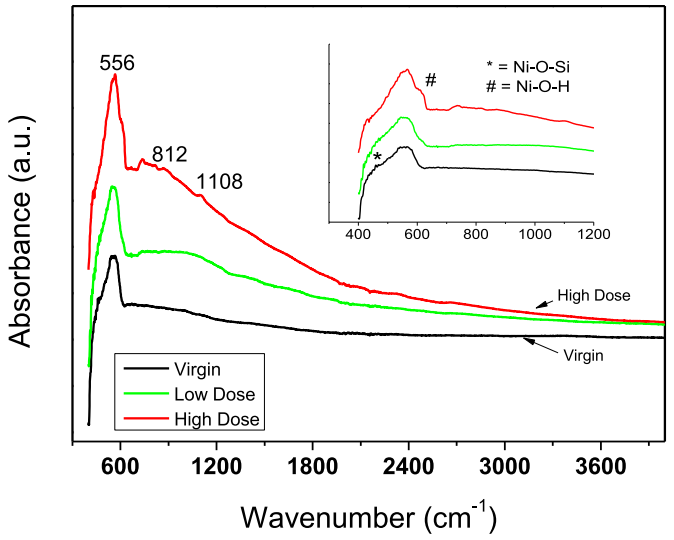

Fig. 3. FTIR spectrocopy of *NiO* thin films with various radiation doses.

appeared at 812 and 1108 cm^{-1}, respectively. The vibration modes around 800 cm^{-1} are associated with non-stoichiometric *Si–O* vibrations. Considering the observed variations in the *FTIR* spectra, it may be concluded that irradiation primarily breaks *Ni–O–Si* bonds, leaving sub-oxide bonds associated with *Ni–O* and *Si–O* stretching.

3.3. Irradiation effects on optical characteristics

In order to examine the effects of radiation on the optical band gap of NiO thin films before and after exposure, the reflectance *(R)* as a function of photon energy, depicted in Fig. 4a, was measured. The highest reflection level was observed around 315 nm wavelength. The reflectance characteristics exhibited a gradual variation in reflectance levels, with a shift towards higher wavelengths following irradiation exposure. This change in reflectance may be attributed to radiation-induced alterations in surface morphology and the formation of crystal defects in the film structure (Saha et al., 2018). In addition, the optical energy gap E_g before and after irradiation with different doses were extracted from the reflectance spectra using the Kubelka–Munk function(Zarrin et al., 2019). The relationship based on the reflectance measurements can be

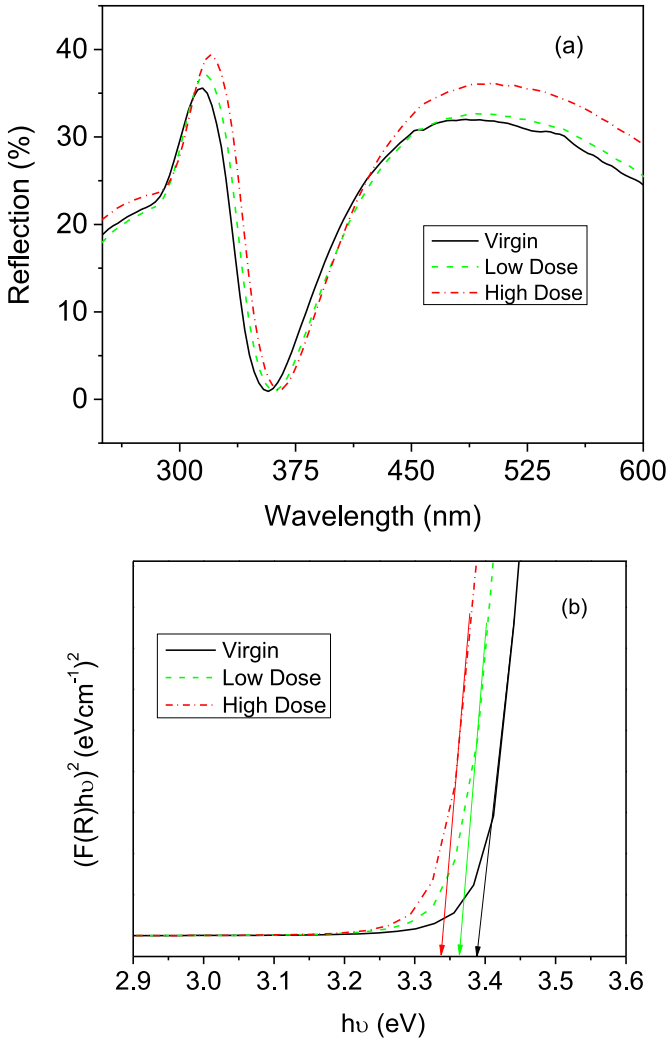

Fig. 4. (a) The reflection spectra, and (b) $(F(R)h\upsilon)^2 - h\upsilon$ curves of NiO thin films before and after the different radiation exposures.

defined in Eq. 1a and b (Kaya, 2020).

$$K/S = (1-R)^2/2R = F(R) \quad (1a)$$

$$F(R) = (1-R)^2/2R \quad (1b)$$

Here, the Kubelka-Munk function is defined as *F(R)*, the *h* is Planck's constant, ν is the frequency of light, $h\nu$ is the photon energy, and *n* is a number representing the type of electronic transition. The E_g is

determined from the plots of $(F(R)h\upsilon)^{1/n}$ versus $h\upsilon$, where E_g corresponds to the intercept at $(F(R)h\upsilon)^{1/n} = 0$. In this case, n is equal to ½, indicating a direct band gap for NiO. The curves of $(F(R)h\upsilon)^2$ versus $h\upsilon$ were presented in Fig. 4b, and the corresponding E_g values were tabulated in Table 1.

Radiation exposure can significantly alter the physical and chemical properties of materials, often leading to the creation of various defects, such as vacancies, interstitial atoms, and other disruptions in the crystal structure (Bai and Uberuaga, 2013). For instance, gamma radiation can modify chemical bonds by breaking Ni–O–Si linkages, which subsequently affects the stretching vibrations of both Ni–O and Si–O bonds. When radiation affects the material, the weak *Ni–O–Si* bonds disappear, while the vibration modes of *Ni–O* and *Si–O* bonds become more pronounced, indicating the presence of new bonds as confirmed by the *FTIR* analysis. Additionally, the peak shifts and broadening observed in *XRD* are also related to these structural changes. These newly formed components introduce localized states within the band gap, facilitating electron transitions at lower energy levels and effectively narrowing the band gap. The Tauc region represents band-to-band transitions characterized by a high energy band gap, which aligns with the higher band gap values observed in non-irradiated samples. In contrast, the Urbach region is associated with energy levels that form at the edges of the conduction and valence bands, extending beyond the primary band structures. Radiation-induced defects and disorders are primarily responsible for these energy levels, leading to the broadening of the conduction and valence bands towards the band gap, a phenomenon known as band tailing(Bouderbala et al., 2024; Hassanien and Sharma, 2019). This effect reduces the observed band gap energy, influencing the material's interaction with photons and altering its optical properties, particularly in the lower band gap range. As depicted in Fig. 5, transitions within the Urbach region can occur from the valence band to a defect state or from a defect state to the conduction band, requiring less energy compared to transitions in the Tauc region(Shahcheragh et al., 2023). Lastly, the *WAT* (Wide Area Transitions) regions, also illustrated in Fig. 5, represents the lowest energy transitions, where transitions occur directly between defect states (Bouderbala et al., 2024; Hassanien et al., 2020; Shahcheragh et al., 2023)Based on these observations, the decrease in E_g with increasing radiation dose is attributed to defect-related transitions (Abubakar et al., 2017)within the band of *NiO*.

3.4. Irradiation effects on electrical characteristics of p-NiO/n-Si

Sheet resistance (R_{sq}) of thin films uniformly thick and was used to evaluate the electrical properties of these materials. The irradiation induced effects on the R_{sq} value were measured via four-point probe methods and tabulated in Table 2. The R_{sq} slightly decreased from 65.2 Ω-cm to 64.4 Ω-cm after high dose exposure. *NiO* is recognized as a wide band gap semiconductor, and its p-type conductivity is associated with neutral non-stoichiometric defects, particularly nickel vacancies that form acceptor impurities, within its structure (Thimsen et al., 2012). As the irradiation dose increased, the formation of new defect centers can create additional defect sites that may contribute to conduction. Thus, the decrease in R_{sq} values might be attributed to defect formation induced by irradiation. In the other words, gamma irradiation affects the *p-NiO/n-Si* heterojunction by generating defects that act as trapping and recombination centers, altering charge carrier dynamics. These defects may release free carriers upon ionization, leading to an increase in carrier concentration, while also introducing scattering centers that may reduce mobility. In this study, the observed decrease in sheet resistance with increasing irradiation doses may suggest that the rise in carrier concentration outweighs the reduction in mobility, reflecting a net enhancement in conductivity (decrease in R_{sq}) due to radiation exposure. Consequently, both defect formation and structural changes contribute to an overall increase in the material's electrical conductivity, resulting in a decrease in the R_{sq}.

The *I–V* characteristics of the *p-NiO/n-Si* heterojunction diode was shown in Fig. 6. With the increase in radiation dose, the diode's turn-on voltage shifted to more positive values. In the semi-logarithmic coordinate system, the minimum current should occur at the point where the voltage is nearly zero. However, in the heterojunction diode's log-scale *I–V* curve shown in the figure, the voltage where the current sharply drops almost zero Ampere shifted toward more positive voltages. This shift may be attributed to either the rises in leakage current of the device

Table 2
Some electrical parameters of *p-NiO/n-Si* heterojunction diodes.

Sample	R_{sq} (Ω/sq)	I_f/I_r	R_s (kΩ)	R_{sh} (MΩ)	n	I_o (nA)	ϕ_b (eV)
Virgin	65.2	78.4	37.1	39.7	1.64	8.09	0.79
Low D.	65.0	51.2	40.5	41.4	1.66	2.15	0.82
High D.	64.4	18.4	144	147	1.83	0.31	0.87

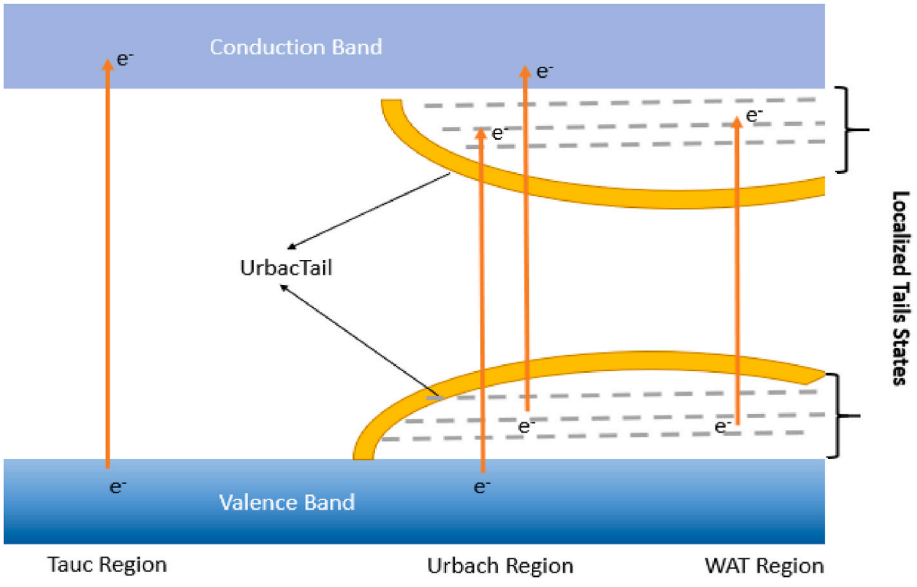

Fig. 5. General conditions that may arise from radiation in the valence and conduction band gaps of semiconductor devices.

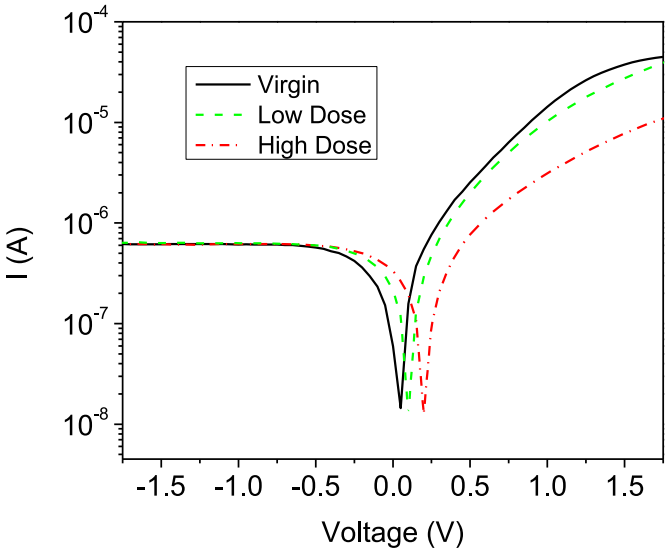

Fig. 6. The I–V curves of the *p-NiO/n-Si* heterojunction diodes before and after various radiation doses.

or the formation of hysteresis loops, which result in the creation of trapping centers within the devices after irradiation exposures. In the virgin state, the current under reverse bias is quite low, and, as in an ideal diode, the reverse current must be negligible. This indicates that the p-n junction is of high quality and has a low defect density. Under forward bias, the current increases rapidly, which shows that the p-n junction is functioning properly and carrier conduction is occurring efficiently. When examining the effects of radiation, it is observed that there is no significant change in the current under reverse bias. This can be explained by the presence of metal-oxide induced defects, which limit the generation of radiation-induced minority carriers (holes) responsible for the reverse current (Oeba et al., 2024). It is likely that the defects contributions effectively suppress the accumulation of minority carriers caused by radiation. As a result, even with an increase in radiation dose, the current under reverse bias remains almost constant. On the other hand, under forward bias, the current decreases as the radiation dose increases. This indicates that radiation creates defects and trapping centers in the semiconducting oxide materials. Radiation-induced defects act as recombination centers for carriers at the p-n junction and create alternative pathways for electron and hole carriers. This leads to an increase in recombination of carriers and results in a decrease in forward current. Additionally, these defects may cause disruptions in the crystal structure of the oxides, negatively affecting its conductivity properties. In conclusion, the effects of radiation on the semiconducting oxide materials manifest as a decrease in forward current and an increase in carrier recombination (Oeba et al., 2024; Sze et al., 2021).

Additionally, the rectifying behavior, $RF = I_f/I_r$ *at the* ± 1 *V,* of the diodes exhibited variations depending on the irradiation doses as listed in Table 2. A high *RF* value indicated a strong rectifying behavior, meaning the diode conducts much better in the forward direction compared to the reverse direction. A decrease in *RF* values demonstrates that formation of the radiation induced leak path where the carriers may flow and contributed the conduction. Shunt *(Rsh)* and series resistance (R_s) values of heterojunction diodes were also measured to investigated the electrical properties of the samples. The *Rsh* is related to the defect densities at the interface between two semiconductors and surface inhomogeneities, while the *Rs* is generally the resistance arising from the bulk materials of the diode and metallic connections and its interface with diode materials (Kaya and Yilmaz, 2019). The changes in these two quantities due to radiation were tabulated in Table 2. Resistivity is related to the scattering caused by dislocations, impurities within the crystallite, and the potential barrier resulting from the effects of intra-crystallite boundaries, as well as scattering at the nano-crystallite boundaries(Kaya and Yilmaz, 2019). Broken stoichiometric bonds owing to irradiation and formation of the sub-oxide bonds associated with Ni–O and Si–O may cause additional carrier scattering sites during the carrier drift. Variations in the crystalline structure of the materials were also observed in the *XRD* analysis. Hence, enhancement of the R_{sh} and R_s may be due to the formation of the additional scattering centers intra-crystallite boundaries of diode materials. The effect of radiation can unfortunately influence different properties in various ways. In this study, the increase in R_s and R_{sh} values with increasing radiation is consistent with the literature. It has been reported that the R_s value, in particular, increased as the radiation dose increased(D. S. et al., 2020; Kaymaz et al., 2021). However, in some cases, it has also been reported that R_s values decreased as the radiation dose increased (Aldawood et al., 2023).

The Thermionic Emission Model illustrates the relationship between the applied voltage and the current flowing through a diode. Under forward bias, the *I–V* curve typically increases exponentially. This model is expressed by the following equation (Kaya, 2020)

$$I = I_0\left[e^{\left(\frac{qV}{nkT}\right)} - 1\right] \tag{2}$$

I_0 represents the reverse saturation current; q denotes the charge; T specifies the ambient temperature in Kelvin; k is Boltzmann's constant; and n is the ideality factor. To neglect the effects of reverse current on the *I–V* curve, the linear portion of the current is examined under condition $V > 3kT/q$. Additionally, the I_0 value can be defined according to the following equation (Kaya, 2020).

$$I_0 = AA^*T^2\left(e^{\left(\frac{-q\Phi_b}{kT}\right)}\right) \tag{3}$$

A^* is known as the Richardson constant, and for n-Si, this value is approximately 112 A $K^{-2}cm^{-2}$. A represents the contact area, while ϕb denotes the barrier potential. Based on the Eqs. 2 and 3, the following equation expressing n can be derived as,

$$\frac{1}{n} = \frac{kT}{q}\left(\frac{d\ln(I)}{dV}\right) \tag{4}$$

The operating principle of diodes is typically shaped around two main mechanisms: thermal transport *(TE)* and tunnelling. *TE* refers to the movement of carriers influenced by temperature and represents the expected behaviour for ideal diodes. Tunnelling, on the other hand, refers to the ability of carriers to pass through an energy barrier and generally becomes dominant in diodes with lower n values or in situations with high energy barriers. The η value is an important parameter in analysing the *I–V* characteristics of a diode, determining its ideal behaviour. When $\eta = 1$, the diode exhibits completely ideal behaviour, indicating that *TE* is dominant. In the range of $1 < \eta < 2$, the diode's behaviour shows some deviation from ideality, suggesting that other mechanisms, such as tunnelling, become also effective. When $\eta > 2$, significant changes in the current transport mechanism is occurred, and effects like defect-assisted tunnelling or space charge current generally become dominant (Verschraegen et al., 2005). The η value calculated in the forward bias region of the diode's *I–V* curve was presented in Table 2, where it is observed to be between 1 and 2. This indicates that as irradiation exposures increased tunnelling the current transport mechanism become more prominent. The ideality factor measures the deviation from ideal thermionic emission theory. Gamma radiation-induced defect states such as interstitials, vacancies, and defect complexes may increase carrier recombination and tunneling processes, which are not accounted for in the ideal theory. A higher η value highlights the effect of generation-recombination (g-r) centers where mobile charges may contribute the conduction (Oeba et al.,

2024). These additional mechanisms increase the ideality factor as they contribute to non-ideal current transport, such as recombination in the depletion region and defect-assisted tunneling. The barrier height in a junction is influenced by the charge distribution near the interface. Gamma-induced defect states can trap charge, altering the electric field in the depletion. This trapped charge modifies the effective work function difference between diode materials, leading to an apparent increase in the barrier height. Radiation-induced defects and flaws in the crystal structure can reduce carrier mobility, and as the flow of minority carriers decreases, the I_0 value also decreases accordingly (Kim et al., 2018; Sharma et al., 2020).

4. Conclusion

As a result, radiation exposure has led to a shift in the *XRD* peaks to the right by balancing the internal strain distribution of the crystal structure. This shift is a consequence of the reorganization of defects and dislocations within the material, resulting in a more homogeneous structure replacing the previous irregular strain configuration. Additionally, radiation exposure has caused the optical band gap of NiO thin films to narrow, leading to the formation of new defect centers that enhance electrical conductivity. The effects of radiation disrupt the electrical properties of the *p*-NiO/n-Si heterojunction diode and contribute to the formation of sub-oxide bonds related to Ni–O and Si–O. These sub-oxide bonds are primary factors contributing to the reduction in band gap energies. Furthermore, the localized states created by radiation have a significant impact on the overall behavior of the device. Moreover, radiation exposure affects the electrical characteristics of the diode, resulting in increased resistance values and the emergence of a more pronounced tunneling mechanism. Specifically, the increase in R_s and R_{sh} values is related to the reduction of carrier mobility due to defects and irregularities. The decrease in I_0 and the increase in the ϕ_b indicate that the defects induced by radiation hinder carrier flow. This situation signifies a deviation from the diode's ideal behavior and the dominance of more complex transport mechanisms.

CRediT authorship contribution statement

Ramazan Lok: Writing – original draft. **Muhsin U. Doğan:** Data curation. **Senol Kaya:** Writing – original draft, Data curation. **Ugur Soykan:** Writing – original draft, Data curation. **Cabir Terzioğlu:** Writing – original draft.

Declaration of competing interest

The authors declare that they have no known competing financial interests or personal relationships that could have appeared to influence the work reported in this paper.

Acknowledgment

This study was partially funded by the Presidency of the Republic of Turkey, Presidency of Strategy and Budget (Contract Number: 2016K12-2834), as well as by BAIBU (Contract Number: 2018.January 34, 1395), with additional support provided by the authors' personal budgets.

Data availability

Data will be made available on request.

References

Abubakar, S., Kaya, S., Aktag, A., Yilmaz, E., 2017. Yttrium oxide nanostructured thin films deposited by radio frequency sputtering: the annealing optimizations and correlations between structural, morphological, optical and electrical properties. J. Mater. Sci. Mater. Electron. 28, 13920–13927. https://doi.org/10.1007/s10854-017-7241-7.

Ahmed, R.M., Sallam, O.I., 2024. Optical properties, FTIR, and electron Spin resonance analysis on the impact of gamma irradiation on fluorophosphate glasses doped with iron (III) oxide. Ceram 50, 31767–31779. https://doi.org/10.1016/j.ceramint.2024.05.364.

Akay, D., Karadeniz, S., Selçuk, A.B., Ocak, S.B., 2018. Effect of gamma-ray irradiation on the electrical characteristics of Al/C24H12/p-Si nano-structure. Phys Scr 93, 095301.

Akila, T., Gayathri, P., Alan Sibu, G., Balasubramani, V., Al-Lohedan, H., Al-Dhayan, D. M., 2024. Augmented photovoltaic performance of Cu/Ce-(Sn:Cd)/n-Si Schottky barrier diode utilizing dual-doped Ce-(Sn:Cd) thin films. Opt. Mater. 149, 115133. https://doi.org/10.1016/j.optmat.2024.115133.

Al-Ahmadi, N.A., 2020. Metal oxide semiconductor-based Schottky diodes: a review of recent advances. Mater. Res. Express 7, 032001.

Alagiri, M., Ponnusamy, S., Muthamizhchelvan, C., 2012. Synthesis and characterization of NiO nanoparticles by sol–gel method. J. Mater. Sci. Mater. Electron. 23, 728–732.

Aldawood, S., Bannoob, W.M., Ali, S.M., 2023. Impact of gamma rays on the structural, optical, and current-voltage characteristics of CuPbI3/p-Si heterojunctions. Mater. Chem. Phys. 309. https://doi.org/10.1016/j.matchemphys.2023.128420.

Ashery, A., Elnasharty, M.M.M., Hameed, T.A., 2020. Investigation of electrical and dielectric properties of epitaxially grown Au/n-GaAs/p-Si/Al heterojunction. Opt Quantum Electron 52, 490.

Ata-ur-Rehman, Iftikhar, M., Latif, S., Jevtovic, V., Ashraf, I.M., El-Zahhar, A.A., Abdu Musad Saleh, E., Mustansar Abbas, S., 2022. Current advances and prospects in NiO-based lithium-ion battery anodes. Sustain. Energy Technol. Assessments. https://doi.org/10.1016/j.seta.2022.102376.

Bai, X.M., Uberuaga, B.P., 2013. The influence of grain boundaries on radiation-induced point defect production in materials: a review of atomistic studies. JOM 65, 360–373. https://doi.org/10.1007/s11837-012-0544-5.

Bilgili, A.K., Güzel, T., Özer, M., 2019. Current-voltage characteristics of Ag/TiO2/n-InP/Au Schottky barrier diodes. J. Appl. Phys. 125.

Bobby, A., Shiwakoti, N., Verma, S., Gupta, P.S., Antony, B.K., 2014. Enhancement in electrical properties of Au/n-GaAs Schottky diodes exposed to 60Co gamma rays. Mater. Sci. Semicond. Process. 21, 116–121. https://doi.org/10.1016/j.mssp.2014.01.039.

Bodunrin, J.O., Moloi, S.J., 2022. Current-voltage characteristics of 4 MeV proton-irradiated silicon diodes at room temperature. Silicon 14, 10237–10244.

Bouderbala, I.Y., Guessoum, A., Rabhi, S., Bouhlassa, O., Bouras, I.-E., 2024. Optical band-diagram, Urbach energy tails associated with photoluminescence emission in defected ZnO thin films deposited by sol–gel process dip-coating: effect of precursor concentration. Appl. Phys. A 130, 205.

Chaoudhary, S., Dewasi, A., S, R.P., Rastogi, V., Pereira, R.N., Sinopoli, A., Aïssa, B., Mitra, A., 2022. Laser ablation fabrication of a P-NiO/N-Si heterojunction for broadband and self-powered UV–Visible–NIR photodetection. Nanotechnology 33, 255202. https://doi.org/10.1088/1361-6528/ac5ca6.

Debelle, A., Declemy, A., 2010. XRD investigation of the strain/stress state of ion-irradiated crystals. Nucl. Instrum. Methods Phys. Res. B 268, 1460–1465.

Dhas, S.D., Maldar, P.S., Patil, M.D., Nagare, A.B., Waikar, M.R., Sonkawade, R.G., Moholkar, A.V., 2020. Synthesis of NiO nanoparticles for supercapacitor application as an efficient electrode material. Vacuum 181. https://doi.org/10.1016/j.vacuum.2020.109646.

Gayathri, P., Akila, T., Sibu, G.A., Selvaraj, M., Assiri, M.A., matheswaran, P., Balasubramani, V., 2024a. Enhancing photovoltaic applications through precipitating agents in ITO/CIS/CeO2/Al heterojunction solar cell. Inorg. Chem. Commun. 168, 112866. https://doi.org/10.1016/j.inoche.2024.112866.

Gayathri, P., Akila, T., Sibu, G.A., Selvaraj, M., Assiri, M.A., matheswaran, P., Balasubramani, V., 2024b. Enhancing photovoltaic applications through precipitating agents in ITO/CIS/CeO2/Al heterojunction solar cell. Inorg. Chem. Commun. 168, 112866. https://doi.org/10.1016/j.inoche.2024.112866.

Gomaa, M.M., Sayed, M.H., Patil, V.L., Boshta, M., Patil, P.S., 2021. Gas sensing performance of sprayed NiO thin films toward NO2 gas. J. Alloys Compd. 885. https://doi.org/10.1016/j.jallcom.2021.160908.

Guo, S., Wang, Y., Qu, H., Zhou, W., Ang, Y.S., Zhang, S., Zeng, H., 2024. Theoretical dissection of the electronic anisotropy and quantum transport of ultrascaled halogenated borophene MOSFETs. Phys. Rev. Appl. 21, 054016.

Hanini, F., Bouabellou, Y., Kermiche, F., Taabouche, A., Hemissi, M., Lakhdari, D., 2013. Structural, optical and electrical properties of TiO2 thin films synthesized by sol–gel technique. IOSR J. Eng. 3, 21–28. https://doi.org/10.9790/3021-031112128.

Hassanien, A.S., Sharma, I., 2019. Band-gap engineering, conduction and valence band positions of thermally evaporated amorphous Ge15-x Sbx Se50 Te35 thin films: influences of Sb upon some optical characterizations and physical parameters. J. Alloys Compd. 798, 750–763.

Hassanien, A.S., Neffati, R., Aly, K.A., 2020. Impact of Cd-addition upon optical properties and dispersion parameters of thermally evaporated CdxZn1-xSe films: discussions on bandgap engineering, conduction and valence band positions. Optik 212, 164681.

Hwang, J., Hwang, Y.-T., 2020. Enhancing ultraviolet-to-visible rejection ratio by inserting an intrinsic NiO layer in P-NiO/N-Si heterojunction photodiodes. Nanotechnology 31, 345205. https://doi.org/10.1088/1361-6528/ab92ca.

Irwin, M.D., Servaites, J.D., Buchholz, D.B., Leever, B.J., Liu, J., Emery, J.D., Zhang, M., Song, J.H., Durstock, M.F., Freeman, A.J., Bedzyk, M.J., Hersam, M.C., Chang, R.P. H., Ratner, M.A., Marks, T.J., 2011. Structural and electrical functionality of NiO interfacial films in bulk heterojunction organic solar cells. Chem. Mater. 23, 2218–2226. https://doi.org/10.1021/cm200229e.

Jabbar, S., Asif, H., Ahmad, R., Sharif, S., Khan, I.A., Shafique, M.A., 2024. Changes in structural and optical properties of TiO2 thin films irradiated by various doses of 300 keV carbon ions. J. Mater. Eng. Perform. 33, 6014–6023.

Kahraman, A., Mutale, A., Lok, R., Yilmaz, E., 2022. Effect of high-radiation-dose-induced structural modifications of HfSiO4/n-Si on electrical characteristics. Radiat. Phys. Chem. 196. https://doi.org/10.1016/j.radphyschem.2022.110138.

Kalkan, Y., 2025. Assessing the shielding capability of NiO-infused BPSCCO ceramics against low-energy X-rays. Ceram. Int. 51, 154–164. https://doi.org/10.1016/j.ceramint.2024.10.388.

Karataş, Ş., Türüt, A., 2006. Electrical properties of Sn/p-Si (MS) Schottky barrier diodes to be exposed to 60Co γ-ray source. Nucl. Instrum. Methods Phys. Res. 566, 584–589.

Kaya, S., 2020. Nanostructure, optical and electrical properties of p-NiO/n-Si heterojunction diodes. Appl. Phys. Mater. Sci. Process 126. https://doi.org/10.1007/s00339-020-03816-8.

Kaya, S., Yilmaz, E., 2018. Modifications of structural, chemical, and electrical characteristics of Er2O3/Si interface under Co-60 gamma irradiation. Nucl. Instrum. Methods Phys. Res. B 418, 74–79. https://doi.org/10.1016/j.nimb.2018.01.010.

Kaya, S., Yilmaz, E., 2019. Effects of interfacial layer on the electrical properties of n-ZnO/p-Si heterojunction diodes between 260 and 340 K. J. Mater. Sci. Mater. Electron. 30, 12170–12179. https://doi.org/10.1007/s10854-019-01575-8.

Kaya, S., Yıldız, I., Lok, R., Yılmaz, E., 2018. Co-60 gamma irradiation influences on physical, chemical and electrical characteristics of HfO2/Si thin films. Radiat. Phys. Chem. 150, 64–70. https://doi.org/10.1016/j.radphyschem.2018.04.023.

Kaya, S., Abubakar, S., Yilmaz, E., 2019. Co-60 gamma irradiation influences on device characteristics of n-SnO2/p-Si heterojunction diodes. Nucl. Instrum. Methods Phys. Res. B 445, 63–68. https://doi.org/10.1016/j.nimb.2019.03.013.

Kaymaz, A., Evcin Baydilli, E., Uslu Tecimer, H., Altındal, Ş., Azizian-Kalandaragh, Y., 2021. Evaluation of gamma-irradiation effects on the electrical properties of Al/(ZnO-PVA)/p-Si type Schottky diodes using current-voltage measurements. Radiat. Phys. Chem. 183. https://doi.org/10.1016/j.radphyschem.2021.109430.

Khorsand Zak, A., Abd Majid, W.H., Abrishami, M.E., Yousefi, R., 2011. X-ray analysis of ZnO nanoparticles by Williamson–Hall and size–strain plot methods. Solid State Sci. 13, 251–256. https://doi.org/10.1016/j.solidstatesciences.2010.11.024.

Kim, H., Kumar, M., Joondong, K., 2018. Improved broadband photoresponse in Schottky-like junction using carrier selective NiO contact on *p*-Si. Sol. RRL 2. https://doi.org/10.1002/solr.201800138.

Lök, R., 2024. Investigation of interface states, series resistance and barrier height variation with frequency in Al/WO3/p-Si (MOS) capacitors. Iğdır Üniversitesi Fen Bilimleri Enstitüsü Dergisi 14, 1538–1549. https://doi.org/10.21597/jist.1529537.

Lok, R., Karacali, H., Varol, A., Camli, U., Yilmaz, E., 2022. Fabrication and characterization of resistance temperature detector by smart mask design. Int. J. Adv. Manuf. Technol. 122, 147–158. https://doi.org/10.1007/s00170-022-09041-2.

Madiba, I.G., Émond, N., Chaker, M., Thema, F.T., Tadadjeu, S.I., Muller, U., Zolliker, P., Braun, A., Kotsedi, L., Maaza, M., 2017. Effects of gamma irradiations on reactive pulsed laser deposited vanadium dioxide thin films. Appl. Surf. Sci. 411, 271–278. https://doi.org/10.1016/j.apsusc.2017.03.131.

Mande, V.K., Kounsalye, J.S., Vyawahare, S.K., Jadhav, K.M., 2019. Effect of γ-radiation on structural, morphological, magnetic and dielectric properties of Zn–Cr substituted nickel ferrite nanoparticles. J. Mater. Sci. Mater. Electron. 30, 56–68.

Mirzayev, M.N., Jabarov, S.H., Asgerov, E.B., Mehdiyeva, R.N., Thabethe, T.T., Biira, S., Tiep, N.V., 2018. X-ray diffraction and thermodynamics kinetics of SiB6 under gamma irradiation dose. Silicon 11, 2499–2504. https://doi.org/10.1007/s12633-018-0039-2.

Nasiri-Tabrizi, B., 2014. Thermal treatment effect on structural features of mechano-synthesized fluorapatite-titania nanocomposite: a comparative study. Journal of Advanced Ceramics 3, 31–42. https://doi.org/10.1007/s40145-014-0090-4.

Oeba, D.A., Bodunrin, J.O., Moloi, S.J., 2024. Enhancing radiation-hardness of Si-based diodes: an investigation of Al-doping effects in Si using I–V measurements. Radiat. Phys. Chem. 223, 111873. https://doi.org/10.1016/j.radphyschem.2024.111873.

Omotoso, E., Meyer, W.E., Auret, F.D., Paradzah, A.T., Diale, M., Coelho, S.M.M., van Rensburg, P.J.J., 2015. The influence of high energy electron irradiation on the Schottky barrier height and the Richardson constant of Ni/4H-SiC Schottky diodes. Mater. Sci. Semicond. Process. 39, 112–118.

Omran, M., Fabritius, T., Elmahdy, A.M., Abdel-Khalek, N.A., El-Aref, M., Elmanawi, A. E.-H., 2015. XPS and FTIR spectroscopic study on microwave treated high phosphorus iron ore. Appl. Surf. Sci. 345, 127–140. https://doi.org/10.1016/j.apsusc.2015.03.209.

Pai, S.H.S., Pandey, S.K., Samuel, E.J.J., Jang, J.U., Nayak, A.K., Han, H.S., 2024. Recent advances in NiO-based nanostructures for energy storage device applications. J. Energy Storage. https://doi.org/10.1016/j.est.2023.109731.

Parks, J.E., 2015. The Compton effect-Compton scattering and gamma ray spectroscopy. Department of Physics and Astronomy. The University of Tennessee, Knoxville. Tennessee 31200–37996.

Pastuovic, Z., Vittone, E., Siegele, R., Ohshima, T., Iwamoto, N., Forneris, J., Cohen, D.D., Capan, I., 2014. Radiation Hardness of N-type SiC Schottky Diodes.

Paul, M.J., Suresh, R., Gayathri, P., Balasubramani, V., Al-Anazi, K.M., Farah, M.A., 2024. CuO-La2O3 composite-enabled mis Schottky barrier diodes: a novel approach to optoelectronic device diversification. J. Inorg. Organomet. Polym. Mater. https://doi.org/10.1007/s10904-024-03277-z.

Pillai, V.R.V., Khamari, S.K., Dixit, V.K., Ganguli, T., Kher, S., Oak, S.M., 2012. Effect of γ-ray irradiation on breakdown voltage, ideality factor, dark current and series resistance of GaAs p–i–n diode. Nucl. Instrum. Methods Phys. Res. 685, 41–45.

Rattana, T., Suwanboon, S., Kedkaew, C., Wanichchang, K., Choeysuppaket, A., 2016. Effect of annealing temperature on NiO/ZnO heterojunction thin films prepared by sol-gel method. Key Eng. Mater. 675–676, 225–228. https://doi.org/10.4028/www.scientific.net/kem.675-676.225.

Riahi, R., Derbali, L., Ouertani, B., Ezzaouia, H., 2017. Temperature dependence of nickel oxide effect on the optoelectronic properties of porous silicon. Appl. Surf. Sci. 404, 34–39. https://doi.org/10.1016/j.apsusc.2017.01.197.

Saha, S.M.K., Ali, M.H., Hossen, M.F., Pervez, M.F., Mia, M.N.H., Hossain, M.K., Haque, M.A.S., 2018. Structural, morphological, and optical properties of CuO thin films treated by gamma ray. In: 2018 International Conference on Computer, Communication, Chemical, Material and Electronic Engineering (IC4ME2), pp. 1–4. IEEE.

Sajilal, K., Moses Ezhil Raj, A., 2016. Effect of thickness on physico-chemical properties of p-NiO (bunsenite) thin films prepared by the chemical spray pyrolysis (CSP) technique. Optik 127, 1442–1449. https://doi.org/10.1016/j.ijleo.2015.11.026.

Sayyed, M.I., Elmosalami, T.A., Abdo, M.A., Sadeq, M.S., 2022. Optical and radiation shielding features of NiO-CdO-BaO borosilicate glasses. Phys Scr 97, 085802.

Shahcheragh, S.K., Bagheri Mohagheghi, M.M., Shirpay, A., 2023. Effect of physical and chemical activation methods on the structure, optical absorbance, band gap and urbach energy of porous activated carbon. SN Appl. Sci. 5. https://doi.org/10.1007/s42452-023-05559-6.

Sharma, C., Visvkarma, A.K., Laishram, R., Kumar, A., Rawal, D.S., Vinayak, S., Singh, R., 2020. Effect of γ-ray irradiation on Schottky and ohmic contacts on AlGaN/GaN hetero-structures. Microelectron. Reliab. 105, 113565.

Sivaiah, M.V., Petit, S., Barrault, J., Batiot-Dupeyrat, C., Valange, S., 2010. CO2 reforming of CH4 over Ni-containing phyllosilicates as catalyst precursors. Catal. Today 157, 397–403. https://doi.org/10.1016/j.cattod.2010.04.042.

Smith, B.C., 2018. Infrared Spectral Interpretation: a Systematic Approach. CRC press.

Sze, S.M., Li, Y., Ng, K.K., 2021. Physics of Semiconductor Devices. John wiley & sons.

Teffahi, A., Hamri, D., Mostefa, A., Saïdane, A., Saqri, N.A., Felix, J.F., Henini, M., 2016. Effect of 60Co Γ-ray irradiation on electrical properties of Ti/Au/GaAs1−xNx Schottky diodes. Curr. Appl. Phys. 16, 850–858. https://doi.org/10.1016/j.cap.2016.05.003.

Thimsen, E., Martinson, A.B.F., Elam, J.W., Pellin, M.J., 2012. Energy levels, electronic properties, and rectification in ultrathin P-NiO films synthesized by atomic layer deposition. J. Phys. Chem. C 116, 16830–16840. https://doi.org/10.1021/jp302008k.

Varichenko, V.S., Zaitsev, A.M., Lindner, J.K.N., Domres, R., Penina, N.M., Erchak, D.P., Chelyadinskii, A.R., Martinovitsh, V.A., 1994. EPR, XRD and optical reflectivity studies of radiation damage in silicon after high energy implantation of Ni ions. Nucl. Instrum. Methods Phys. Res. B 94, 240–244.

Verschraegen, J., Burgelman, M., Penndorf, J., 2005. Temperature dependence of the diode ideality factor in CuInS2-on-Cu-tape solar cells. Thin Solid Films 480–481, 307–311. https://doi.org/10.1016/j.tsf.2004.11.006.

Vinila, V.S., Jacob, R., Mony, A., Nair, H.G., Issac, S., Rajan, S., Nair, A.S., Isac, J., 2014. XRD studies on nano crystalline ceramic superconductor PbSrCaCuO at different treating temperatures. Crystal Structure Theory and Applications 03 1–9. https://doi.org/10.4236/csta.2014.31001.

Wang, C., Xu, W., Qi, L., Ding, H., Cai, W., Jiang, G., Hu, Y., Xing, W., Yu, B., 2023. Hierarchical NiO/Al2O3 nanostructure for highly effective smoke and toxic gases suppression of polymer Materials: experimental and theoretical investigation. Compos Part A Appl Sci Manuf 175. https://doi.org/10.1016/j.compositesa.2023.107807.

Yağci, Ö., 2023. Effect of gamma irradiation on structural, morphological, optical and thermal properties of Ca doped CuO nanostructure thin films. Radiat. Eff. Defect Solid 178, 521–538.

Zarrin, N., Husain, S., Khan, W., Manzoor, S., 2019. Sol-gel derived cobalt doped LaCrO3: structure and physical properties. J. Alloys Compd. 784, 541–555. https://doi.org/10.1016/j.jallcom.2019.01.018.

Zhang, D., Nozaki, S., Uchida, K., 2014. NiO/Si heterostructures formed by UV oxidation of nickel deposited on Si substrates. Journal of Vacuum Science & Technology B Nanotechnology and Microelectronics Materials Processing Measurement and Phenomena 32. https://doi.org/10.1116/1.4868634.